Macromolecules

pubs.acs.org/Macromolecules Article

Phenolic Formaldehyde Resin-Based Nano-objects via a Modification-Induced Cooperative Assembly Process Using Poly(4-hydroxystyrene) as the Core-Forming Block

Peng Zhou, Boyang Shi, Jingwei Zhang, Ding Shen, Di Li, Xinyue Liang, and Guowei Wang*

Cite This: *Macromolecules* 2025, 58, 11123−11136 Read Online

ACCESS | Metrics & More | Article Recommendations | Supporting Information

ABSTRACT: Harnessing the preparation and application of nano-objects with defined compositions and functions has much importance in advanced material fields. Although the scalable production of nano-objects has been accelerated by the efficient polymerization-induced self-assembly (PISA) process, more powerful self-assembly processes are still pursued. In this contribution, the modification-induced self-assembly (MISA) of poly(styrene)-*b*-poly(4-hydroxystyrene) (PS-*b*-P*t*BOS) diblock copolymers was studied by employing trifluoroacetic acid (TFA) as a modifying reagent and toluene as a selective solvent. Furthermore, to enrich the morphological formation window and enhance the MISA process, a modification-induced cooperative assembly (MICA) process was derived by synergistically incorporating the PS-*b*-P*t*BOS block copolymers and the P*t*BOS homopolymer into the same system. By comprehensively optimizing the degree of polymerization of P*t*BOS (DP_{PtBOS}) and the P*t*BOS homopolymer content, the morphologies could be modulated in a broad window. Especially, the rarely observed sponge-like morphology was also captured in the MICA system. Additionally, employing the efficient reaction between the phenolic hydroxyl group and formaldehyde, the PHOS core can be stabilized and a phenolic formaldehyde resin-based nano-object could be generated. The MISA or MICA processes greatly facilitated the preparation of nano-objects, which have potential as novel advanced materials.

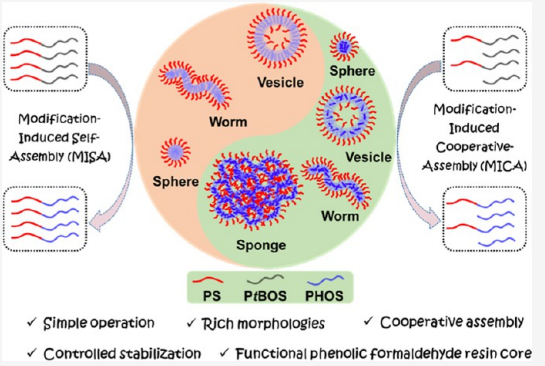

INTRODUCTION

The self-assembly of block copolymers has gained much progress in the past 20 years,[1,2] and the corresponding nano-objects generated by self-assembly have also found extensive practical applications,[3−5] including nanocomposite materials, biomedical materials, batteries, functional coatings, Pickering emulsifiers, nanostructured membranes, hydrogels, luminescent materials, and other fields. Presently, the scalable preparation of nano-objects can be realized by the polymerization-induced self-assembly (PISA) process[6−12] or the derived polymerization-induced cooperative assembly (PICA) process,[13−17] in which the polymerization and self-assembly processes occur simultaneously, starting from a macroinitiator (in PISA) or accompanied by a small initiator (in PICA). Typically, in PISA or PICA processes, the solids content reached up to 50% w/w and the operations were significantly simplified. Essentially, the PISA or PICA processes should be performed in a controlled/"living" polymerization system, such as the reversible addition−fragmentation chain transfer (RAFT) polymerization,[9,11,18−20] atom transfer radical polymerization (ATRP),[21−26] nitroxide-mediated polymerization (NMP),[27−29] ring-opening metathesis polymerization (ROMP),[30−33] living anionic polymerization (LAP),[34−37] and so on. Additionally, for block copolymer containing (semi)-crystalline blocks, the crystallization-driven self-assembly (CDSA) process employing the crystallization as driving force has also emerged as an efficient strategy to obtain the well-defined one-dimensional (1D) and two-dimensional (2D) nano-objects.[38−44] Unavoidably, each process has its own limitations or drawbacks, which narrow the practical applications. To solve the current problems, the self-assembly still requires a more efficient technique, which should have the basic merits of simple operations and high solids content.

Previously, our group developed a modification-induced self-assembly (MISA) technique employing poly(*tert*-butyl acrylate)-*b*-polystyrene (P*t*BA-*b*-PS) diblock copolymer as a research model.[45] In the presence of trifluoroacetic acid (TFA), the P*t*BA could be hydrolyzed into poly(acrylic acid) (PAA) block. Meanwhile, the employed toluene became a selective solvent for the generated PAA-*b*-PS diblock copolymer, inducing an in situ self-assembly process. The

Received: August 11, 2025
Revised: September 22, 2025
Accepted: October 1, 2025
Published: October 13, 2025

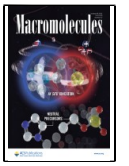

https://doi.org/10.1021/acs.macromol.5c02207
Macromolecules 2025, 58, 11123−11136

practicability of MISA was preliminarily verified, indicating its powerful function for the self-assembly of block copolymers that cannot be prepared by direct polymerization in PISA or PICA processes, as well as the copolymers with complex topologies such as the star-shaped $(A\text{-}b\text{-}B)_n$ or $(B\text{-}b\text{-}A)_n$. Additionally, the residual monomers and catalysts could be completely avoided due to the use of prepurified copolymers. The MISA process could also be realized under mild conditions, unlike those in a "living"/controlled polymerization mechanism, as well as was readily performed with multiple block copolymers or homopolymers by a simple blending process. To delve deeper into the MISA technique, more research models and application scenarios are waiting to be explored.

Poly(4-hydroxystyrene) (PHOS), due to the presence of a phenolic hydroxyl group, is characterized by high polarity. For instance, in a bulk system, polystyrene-*b*-PHOS (PS-*b*-PHOS), a diblock copolymer characterized by a high Flory–Huggins parameter (χ), exhibited the capability to self-assemble into small-sized layered microdomains, rendering it applicable in photoresist technology through the directed self-assembly (DSA) technique.[46] In a solution system, by a conventional self-assembly process, the PS-*b*-PHOS diblock copolymer in a selective solvent of tetrahydrofuran (THF)/toluene mixture underwent morphological changes from spheres to worms or vesicles through the addition of a less favorable solvent of toluene.[47] Although the PHOS-based block copolymers have exhibited powerful self-assembly behavior in bulk or solution systems, the synthesis of PHOS or its derivatives still has many limitations. That is, PHOS cannot be prepared by the direct polymerization of the 4-hydroxystyrene monomer via either a radical polymerization or an ionic polymerization. Alternatively, PHOS must be generated by hydrolysis from a precursor. For instance, Batsberg et al.[48,49] synthesized PHOS by a first atom transfer radical polymerization (ATRP) of a poly(4-acetoxystyrene) (PAcOS) monomer and a subsequent hydrolysis process. Natatello et al.[50] synthesized poly(1-vinyl-4-(1-ethoxyethoxy)benzene)(P(*p*EES)) by a LAP of the *p*EES monomer and finally PHOS by a hydrolysis process. Similarly, Gopalan et al. synthesized PHOS by a LAP of the 4-(2-tetrahydropyranyloxy)styrene (OTHPSt) monomer and a subsequent hydrolysis process. Brinke et al.[51] synthesized PHOS by sequential RAFT polymerization of the 4-*tert*-butoxystyrene (*t*BOS) monomer and a subsequent hydrolysis process. Obviously, the PHOS has distinct solubility with its precursor and an indirect synthesis process,[52,53] endowing PHOS with potential as a research model in the MISA process. Additionally, the PHOS with a phenolic hydroxyl group was also endowed with versatile functions and irreplaceable applications. For example, the PHOS-based copolymers have found extensive applications, including the compatibilizers,[54] adsorbent materials,[55] organic–inorganic composites,[56] and semiconductor resist materials,[57] as well as the potential for the preparation of phenolic formaldehyde resin.

In this work, employing PS-*b*-P*t*BOS diblock copolymers as a research model, TFA as a modifying reagent and toluene as a selective solvent, the PS-*b*-PHOS-based nano-objects were investigated and the MISA process was first involved (Scheme 1). Furthermore, a modification-induced cooperative assembly (MICA) process was introduced by synergistically incorporating the PS-*b*-P*t*BOS block copolymers and P*t*BOS homopolymers into the same system. The comprehensive optimization of the degree of polymerization of P*t*BOS (DP_{PtBOS}) in the

Scheme 1. Synthetic Procedure for the PS-*b*-P*t*BOS Diblock Copolymer and P*t*BOS Homopolymer (a) and the Illustration of the MISA or MICA Processes (b)

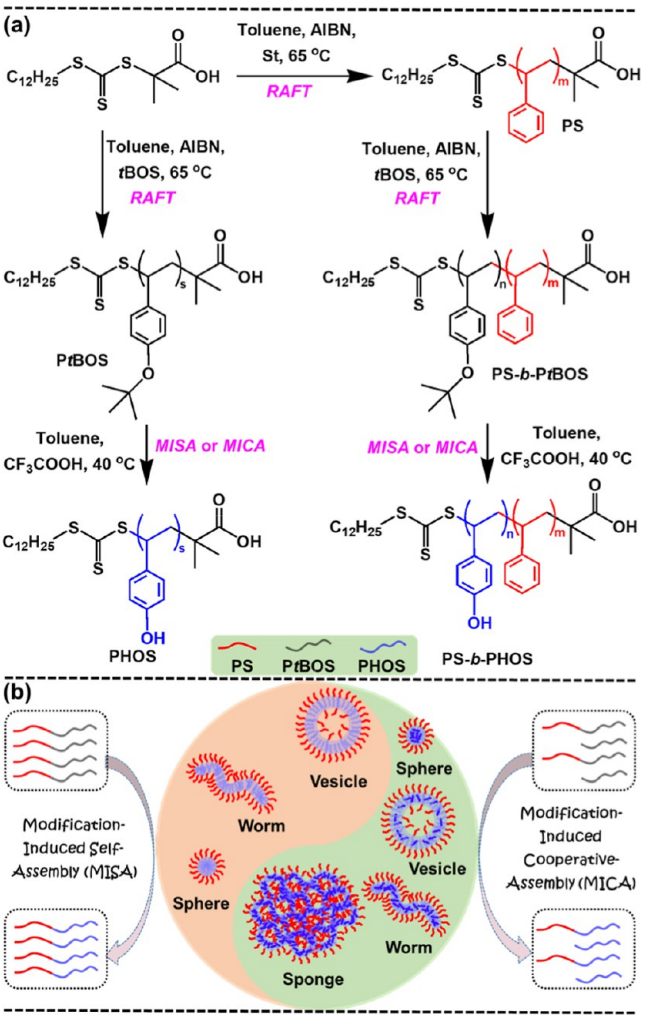

diblock copolymers and homopolymers, and the P*t*BOS homopolymer content, enables the modulation of morphologies in a broad window. Especially, the rarely reported sponge-like morphology was captured in the MICA system. Based on the typical phenol–aldehyde reaction, the nano-objects were finally stabilized by in situ cross-linking of the phenolic hydroxyl groups on the PHOS segment using formaldehyde, and the functional phenolic formaldehyde resin was introduced as the core of the nano-objects. Comprehensively, the composition and structure of the synthesized polymers were characterized via gel permeation chromatography (GPC) and nuclear magnetic resonance spectroscopy (^{1}H NMR) measurements. The morphologies of the resulting nano-objects were assessed through transmission electron microscopy (TEM) and dynamic light scattering (DLS) measurements. Additionally, the thermal stability of the nano-objects was evaluated using thermogravimetric analysis (TGA).

RESULTS AND DISCUSSION

MISA Process for PS-*b*-PHOS Nano-objects. For the MISA process, the macromolecular chain transfer reagent (CTA) of PS_{48}-CTA was first synthesized by RAFT polymerization of the styrene (St) monomer using 2-(dodecylthio-

https://doi.org/10.1021/acs.macromol.5c02207
Macromolecules 2025, 58, 11123–11136

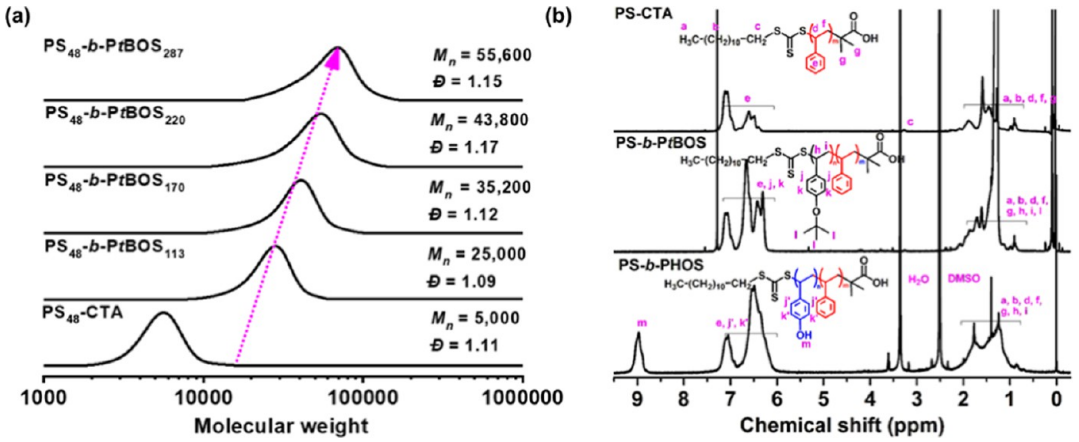

Figure 1. (a) The GPC traces for PS_{48}-CTA and the corresponding PS-*b*-P*t*BOS diblock copolymers (THF was used for elution, and PS was used as the standard) and (b) ^{1}H NMR spectra for PS_{48}-CTA (in $CDCl_3$), the PS_{48}-*b*-P*t*BOS_{113} diblock copolymer (in $CDCl_3$), and the hydrolyzed counterpart of PS_{48}-*b*-$PHOS_{113}$ (in DMSO-d_6).

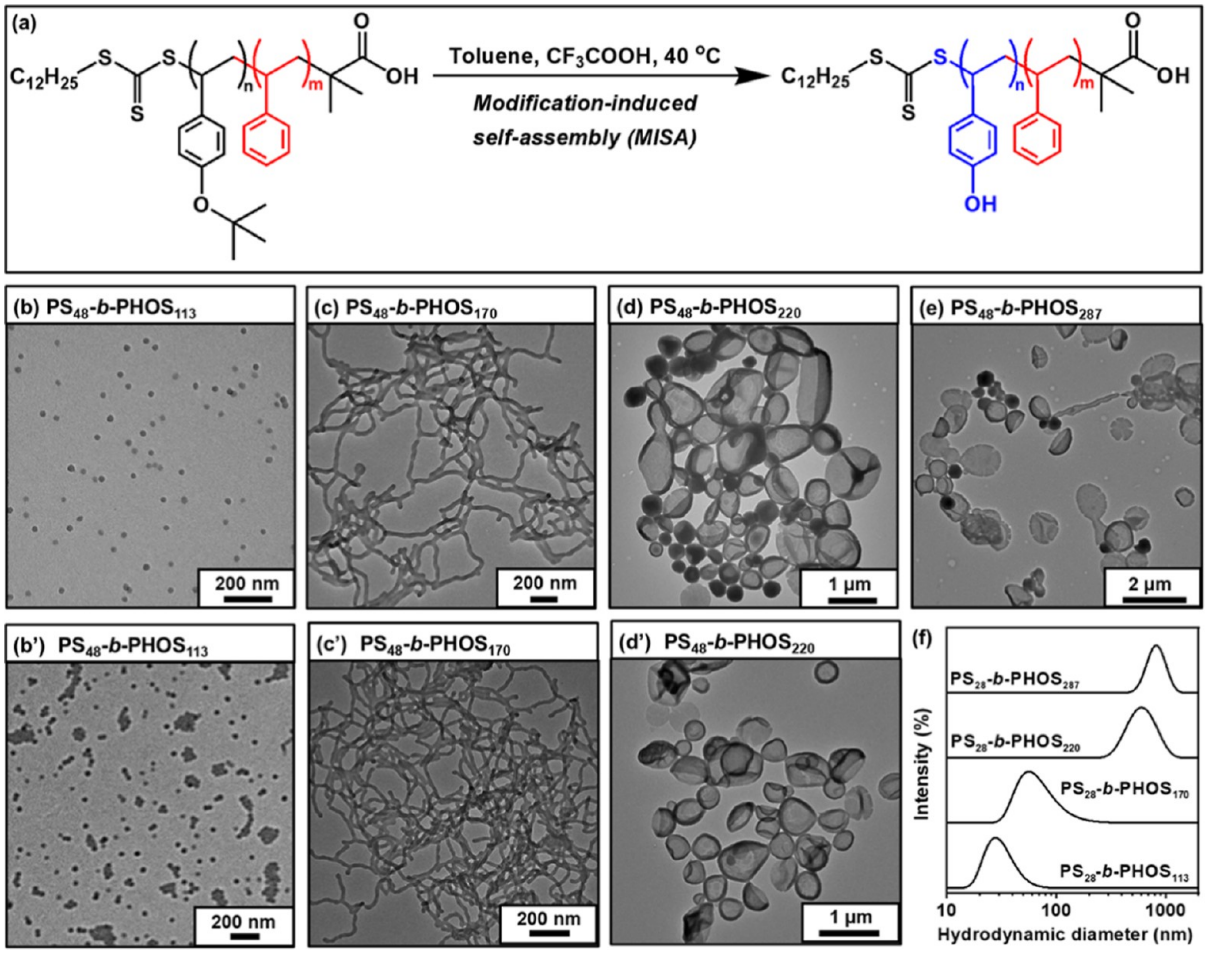

Figure 2. (a) The MISA process for PS-*b*-PHOS diblock copolymers. TEM images of (b, b') PS_{48}-*b*-$PHOS_{113}$, (c,c') PS_{48}-*b*-$PHOS_{170}$, (d, d') PS_{48}-*b*-$PHOS_{220}$, and (e) PS_{48}-*b*-$PHOS_{287}$ nano-objects (diluted into 0.1−0.3% *w*/*w*) formed by the MISA process of PS-*b*-P*t*BOS diblock copolymers with a solids content of 5% *w*/*w*; (b, c, d) and (b', c', d') correspond to the nano-objects before and after the removal of the TFA agent, respectively. (f) The DLS curves of PS-*b*-PHOS nano-objects formed by the MISA process.

carbonothioylthio)-2-methylpropionic acid (DDMAT) as the CTA, 2,2′-azobis(2-methylpropionitrile) (AIBN) as the initiator, and toluene as the solvent. Similarly, the PS-*b*-P*t*BOS diblock copolymers were synthesized through RAFT polymerization of the *tert*-butoxystyrene (*t*BOS) monomer using PS_{48}-CTA as the macromolecular CTA. By adjusting the molar ratio of the *t*BOS monomer to PS_{48}-CTA, the PS-*b*-P*t*BOS diblock copolymers with a fixed degree of polymerization of PS (DP_{PS}) but varying DP of P*t*BOS (DP_{PtBOS}) were obtained. As shown in the GPC curves in Figure 1a, the molecular weights (MWs) of PS-*b*-P*t*BOS diblock copolymers regularly shifted to the higher-MW region with the increase of

https://doi.org/10.1021/acs.macromol.5c02207
Macromolecules 2025, 58, 11123−11136

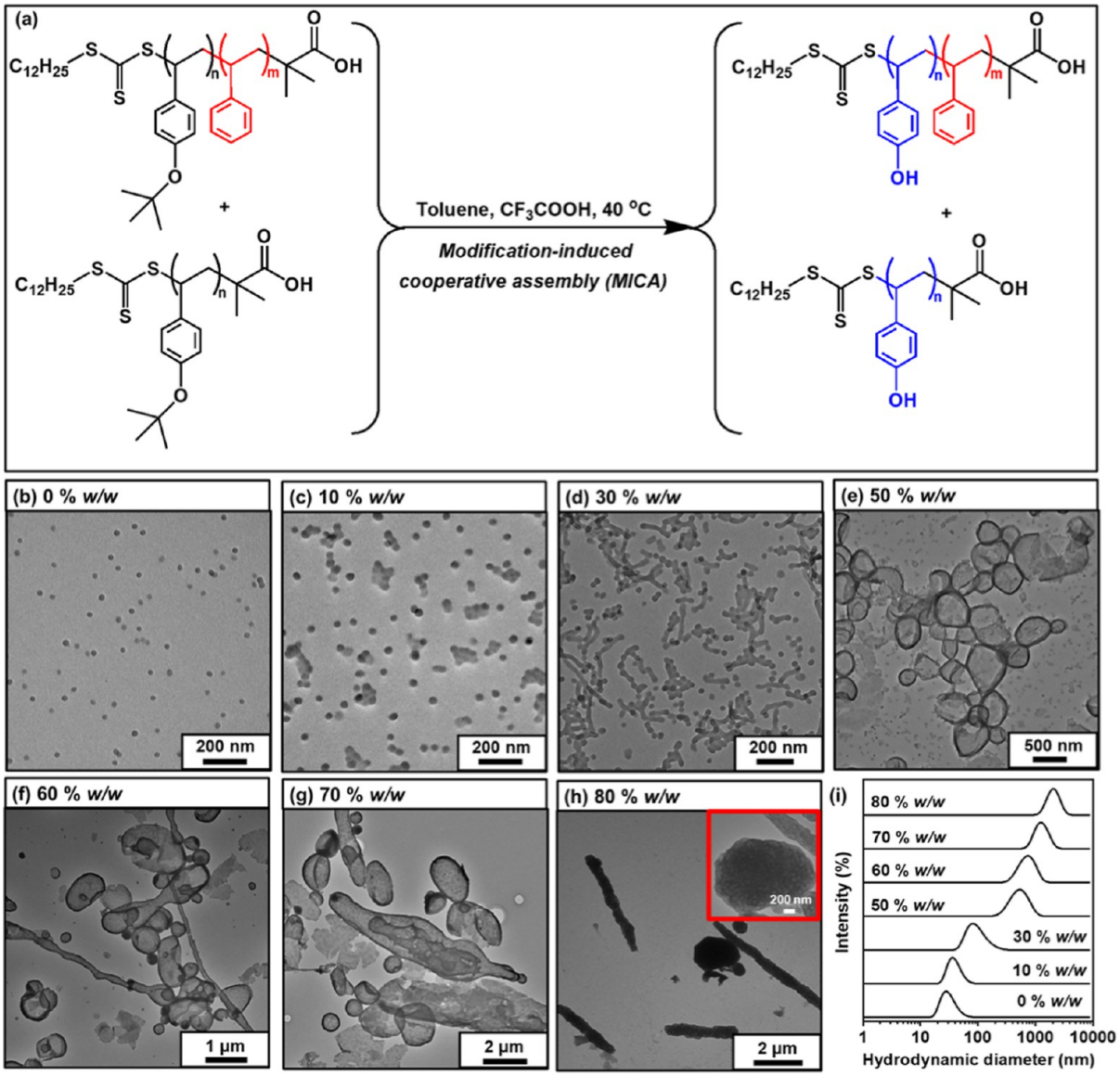

Figure 3. (a) The MICA process for PS-*b*-PHOS/PHOS blends. TEM images of PS_{48}-*b*-$PHOS_{113}$/$PHOS_{28}$ nano-objects (diluted into 0.1−0.3% *w*/*w*) formed by the MICA process of PS_{48}-*b*-P*t*BOS_{113}/P*t*BOS_{28} blends with a solids content of 5% *w*/*w* and different P*t*BOS_{28} homopolymer contents of (b) 0% *w*/*w*, (c) 10% *w*/*w*, (d) 30% *w*/*w*, (e) 50% *w*/*w*, (f) 60% *w*/*w*, (g) 70% *w*/*w*, and (h) 80% *w*/*w*. (i) The DLS curves of nano-objects formed by the MICA process.

DP_{PtBOS}, and the relatively narrow *M*W dispersity ($Đ$ < 1.20) was always maintained. From the ^{1}H NMR spectra for PS_{48}-CTA and PS_{48}-*b*-P*t*BOS_{113} (Figure 1b), the characteristic resonance signals attributed to the benzene protons (−C_6H_4-) on the *t*BOS unit were observed at 6.31 ppm, which overlapped with the benzene protons (−C_6H_5) on the St unit between 6.17 and 7.23 ppm. The *tert*-butyl protons (−OC(CH_3)$_3$) on the *t*BOS unit were discriminated at 1.27 ppm, which overlapped with the methine and methylene protons (−$CHCH_2$-) on the main chain between 0.80 and 2.10 ppm. Based on the fixed DP_{PS}, the DP_{PtBOS}s were derived by comparing the integral areas between 6.17−7.23 and 0.80−2.10 ppm. The GPC and ^{1}H NMR results comprehensively confirmed the successful synthesis of PS-*b*-P*t*BOS diblock copolymers.

Subsequently, the MISA process was carried out by hydrolyzing the P*t*BOS to the PHOS block and converting PS-*b*-P*t*BOS to the PS-*b*-PHOS diblock copolymer, which was performed using toluene as the solvent and TFA as the modification agent (Figure 2a). Typically, toluene was a good solvent for the P*t*BOS block but a poor solvent for the generated PHOS block. Thus, the solubility changes from PS-*b*-P*t*BOS to PS-*b*-PHOS induced an MISA process. Following a similar rule of the PISA system, the variation of DP_{PtBOS} or generated DP_{PHOS} could modulate the morphologies of the generated nano-objects. Regularly, the spherical, worm-like, and vesicular nano-objects were sequentially observed by maintaining PS_{48} as the stabilizer block, increasing the DP_{PHOS}, and fixing the solids content at 5% *w*/*w*. In detail, the PS_{48}-*b*-P*t*BOS_{113} diblock copolymer yielded PS_{48}-*b*-$PHOS_{113}$ and the spherical nano-objects with an average diameter of approximately 20 nm (Figure 2b). The PS_{48}-*b*-P*t*BOS_{170} diblock copolymer formed PS_{48}-*b*-$PHOS_{170}$ and the worm-like nano-objects (Figure 2c). The PS_{48}-*b*-P*t*BOS_{220} and PS_{48}-*b*-P*t*BOS_{287} diblock copolymers formed PS_{48}-*b*-$PHOS_{220}$ and PS_{48}-*b*-$PHOS_{287}$, respectively, as well as the vesicular nano-objects

https://doi.org/10.1021/acs.macromol.5c02207
Macromolecules 2025, 58, 11123−11136

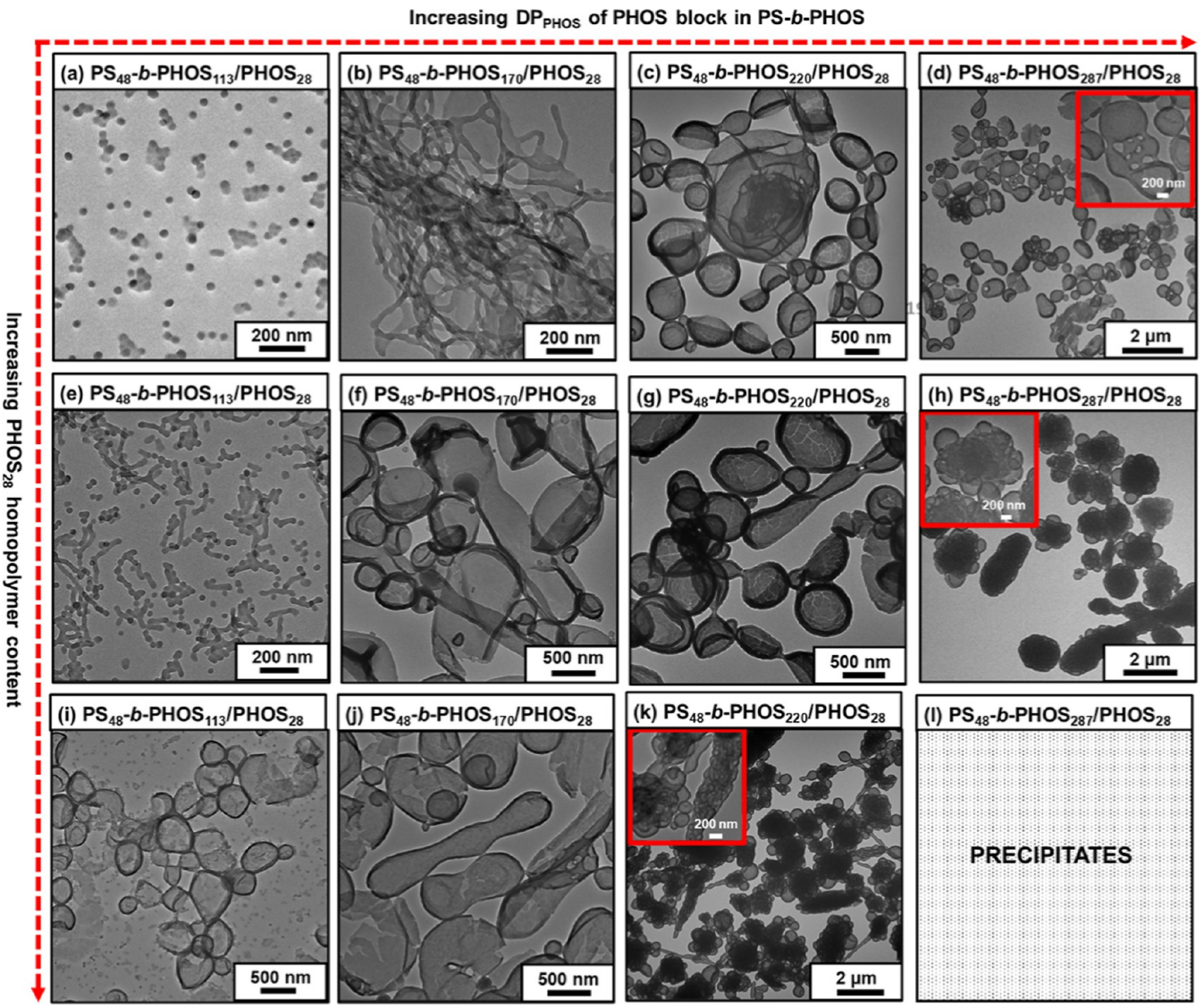

Figure 4. TEM images of PS$_{48}$-*b*-PHOS$_{113}$/PHOS$_{28}$ nano-objects (diluted into 0.1−0.3% *w*/*w*) formed by the MICA process of PS$_{48}$-*b*-P*t*BOS$_{113}$/P*t*BOS$_{28}$, PS$_{48}$-*b*-P*t*BOS$_{170}$/P*t*BOS$_{28}$, PS$_{48}$-*b*-P*t*BOS$_{220}$/P*t*BOS$_{28}$, and PS$_{48}$-*b*-P*t*BOS$_{287}$/P*t*BOS$_{28}$ blends with a solids content of 5% *w*/*w* and different P*t*BOS$_{28}$ homopolymer contents of (a−d) 10% *w*/*w*, (e−h) 30% *w*/*w*, and (i−k) 50% *w*/*w*.

(Figure 2d,e). These results demonstrated that a longer PHOS block promoted the formation of higher-order nano-objects. Meanwhile, the nano-objects in the MISA process were characterized using DLS measurement. As shown in Figure 2f, the PS$_{48}$-*b*-PHOS$_{113}$ system revealed a diameter of around 30 nm and a narrow size distribution. The PS$_{48}$-*b*-PHOS$_{170}$ system showed a diameter of approximately 100 nm and a relatively broad distribution. The PS$_{48}$-*b*-PHOS$_{220}$ system produced vesicular nano-objects with significantly larger diameters, around 700 nm. Similarly, the vesicular nano-objects generated from the PS$_{48}$-*b*-PHOS$_{287}$ system showed a diameter of about 800 nm. The DLS results were consistent with the TEM images, indicating a morphological transition from a lower-order sphere to a higher-order vesicle as the DP$_{PHOS}$ increased. Additionally, as an example, the hydrolyzed product of PS$_{48}$-*b*-PHOS$_{113}$ was characterized by ^{1}H NMR using DMSO-d_6 as a solvent (Figure 1b). Comparing the ^{1}H NMR spectra for PS$_{48}$-*b*-PHOS$_{113}$ with that for the PS$_{48}$-*b*-P*t*BOS$_{113}$ diblock copolymer, the resonance signals attributed to the *tert*-butyl protons (−OC(CH$_3$)$_3$) at 1.30 ppm disappeared. Meanwhile, the resonance signal on the phenolic hydroxyl proton (−C$_6$H$_4$OH) appeared at 8.98 ppm, indicating the successful transformation of P*t*BOS into the PHOS block.

Furthermore, to exclude the effect of the TFA agent, an evaporation process was followed and the TFA agent was selectively removed after the MISA process. The pH value in the MISA system was simultaneously monitored, indicating a shift of the MISA system from the initial acidic to the nearly neutral condition. Meanwhile, a fourier-transform infrared (FTIR) spectrometer was also employed to confirm the successful removal of TFA from the MISA system. As shown in Figure S1, the characteristic peaks of C═ (1750 cm^{-1}) and C−F (approximately 1250−1100 cm^{-1}) attributed to the TFA agent completely vanished after the evaporation process. As shown in Figure 2b'−d', the nano-objects in toluene after the removal of the TFA agent maintained similar morphologies to those in Figure 2b−d, indicating that the TFA agent has a negligible effect on the MISA process. The reason might be the use of a trace amount of the TFA agent. Thus, in the following

https://doi.org/10.1021/acs.macromol.5c02207
Macromolecules 2025, 58, 11123−11136

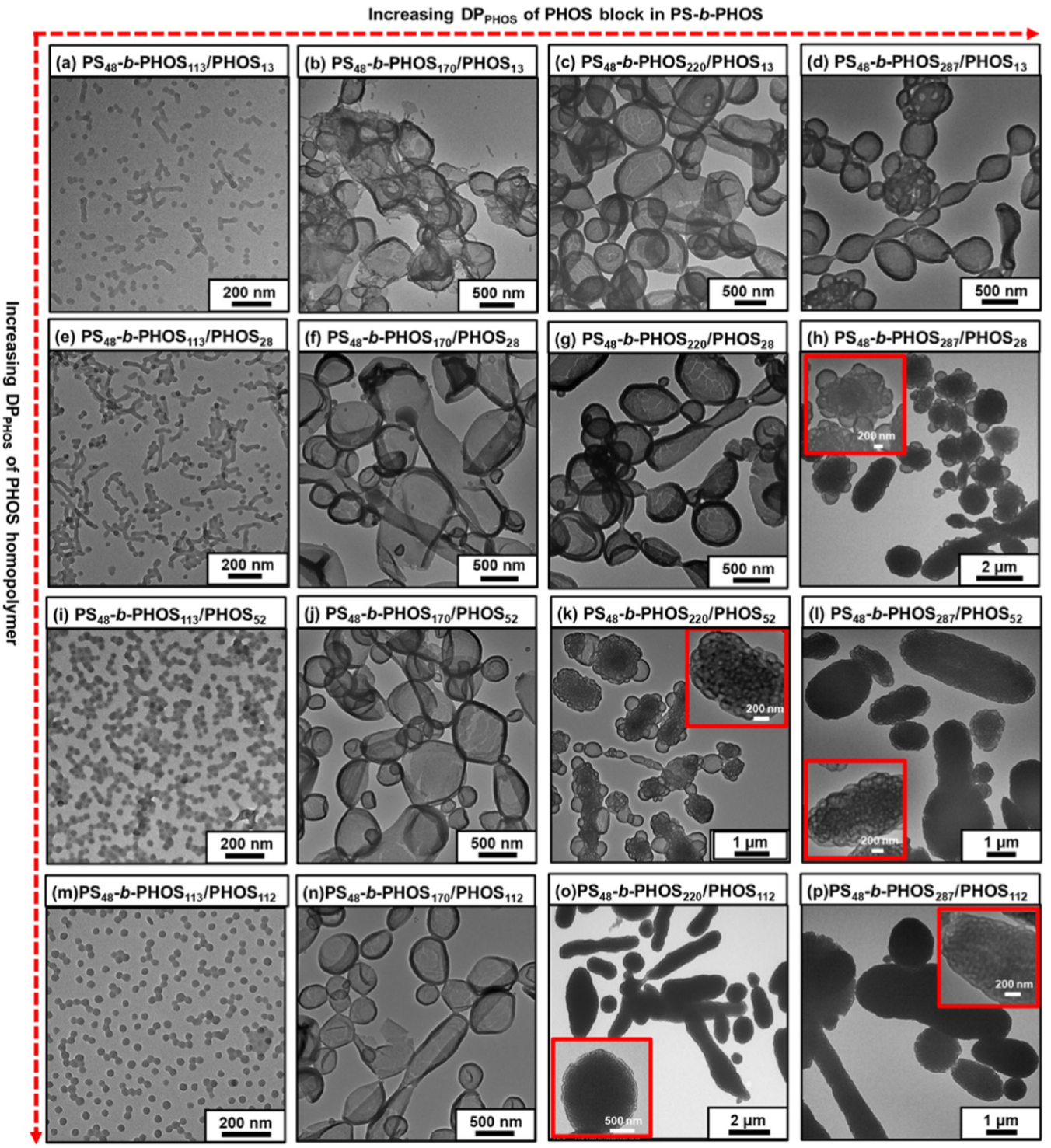

Figure 5. TEM images of nano-objects (diluted into 0.1−0.3% *w*/*w*) formed by the MICA process of PS$_{48}$-*b*-P*t*BOS$_{113}$, PS$_{48}$-*b*-P*t*BOS$_{170}$, PS$_{48}$-*b*-P*t*BOS$_{220}$, and PS$_{48}$-*b*-P*t*BOS$_{287}$ diblock copolymers with 30% *w*/*w* (a−d) P*t*BOS$_{13}$, (e−h) P*t*BOS$_{28}$, (i−l) P*t*BOS$_{52}$, and (m−p) P*t*BOS$_{112}$ homopolymer content and a solids content of 5% *w*/*w*.

works, the nano-objects generated in the MISA process were directly analyzed, and no additional process to remove the TFA agent was performed.

MICA Process for PS-*b*-PHOS/PHOS Nano-objects. As mentioned in the Introduction section, in the conventional self-assembly or PICA process, the addition of a core-forming homopolymer could modulate the morphologies of nano-objects in the self-assembly process of block copolymers. Herein, in our MISA process, the P*t*BOS homopolymer was also introduced into the self-assembly process. Similar to the synthetic process for PS-*b*-P*t*BOS, the P*t*BOS homopolymers with different MWs and relatively low $Đ$ values were synthesized via RAFT polymerization of the *t*BOS monomer by varying the molar ratio of the *t*BOS monomer to DDMAT agent (Figure S2). Consistent with the ^{1}H NMR spectrum for PS$_{48}$-*b*-P*t*BOS$_{113}$, the characteristic resonance signals on

https://doi.org/10.1021/acs.macromol.5c02207
Macromolecules 2025, 58, 11123−11136

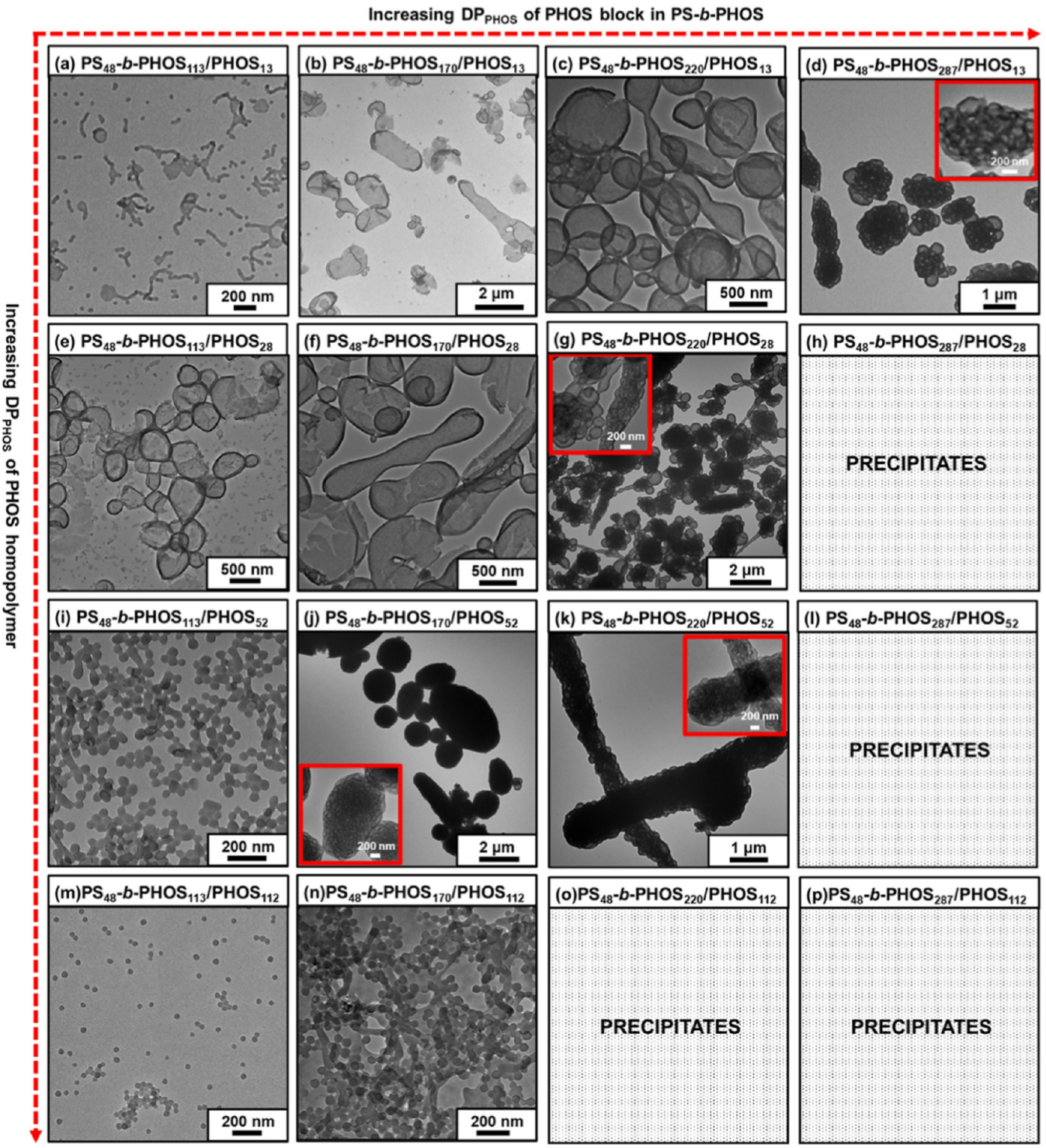

Figure 6. TEM images of nano-objects (diluted into 0.1−0.3% *w*/*w*) formed by the MICA process of PS$_{48}$-*b*-P*t*BOS$_{113}$, PS$_{48}$-*b*-P*t*BOS$_{170}$, PS$_{48}$-*b*-P*t*BOS$_{220}$, and PS$_{48}$-*b*-P*t*BOS$_{287}$ diblock copolymers with 50% *w*/*w* (a−d) P*t*BOS$_{13}$, (e−g) P*t*BOS$_{28}$, (i−k) P*t*BOS$_{52}$, and (m,n) P*t*BOS$_{112}$ homopolymer content and a solids content of 5% *w*/*w*.

P*t*BOS$_{28}$ were also well discriminated (Figure S3). Correspondingly, the MICA process was realized, in which the solids content was also fixed as 5% *w*/*w*, TFA was used as a modification agent, and toluene was used as a solvent (Figure 3a).

First, using the PS$_{48}$-*b*-P*t*BOS$_{113}$/P*t*BOS$_{28}$ blends as a research model, the MICA process was studied by varying the P*t*BOS$_{28}$ homopolymer content from 0% *w*/*w* to 90% *w*/*w*, which was also related to the PHOS$_{28}$ homopolymer content. As shown in Figure 3c, the PS$_{48}$-*b*-P*t*BOS$_{113}$/P*t*BOS$_{28}$ blend with 10% *w*/*w* P*t*BOS$_{28}$ homopolymer generated spherical PS$_{48}$-*b*-PHOS$_{113}$/PHOS$_{28}$ nano-objects, resembling the spherical ones observed in the MISA process from PS$_{48}$-*b*-PHOS$_{113}$ (Figure 3b). Increasing the P*t*BOS$_{28}$ homopolymer content to 30% *w*/*w* resulted in a mixture of spherical and worm-like nano-objects (Figure 3d). Increasing the P*t*BOS$_{28}$ homopol-

https://doi.org/10.1021/acs.macromol.5c02207
Macromolecules 2025, 58, 11123−11136

ymer content to 50% *w*/*w* led to the formation of vesicular nano-objects (Figure 3e). On increasing the $PtBOS_{28}$ homopolymer content to 60% *w*/*w* and 70% *w*/*w*, some unusual tubular vesicles could be discriminated (Figure 3f,g). When the $PtBOS_{28}$ homopolymer content was further increased to 80% *w*/*w*, rod-like aggregates were observed (Figure 3h), internally exhibiting a regular sponge-like morphology. However, at a $PtBOS_{28}$ homopolymer content of 90% *w*/*w*, the system rapidly precipitated within 3.0 h after the MICA process (Figure S4). Meanwhile, the DLS analysis was used to monitor the morphological evolution of nano-objects (Figure 3i). The spherical nano-objects generated from the MISA process of the PS_{48}-*b*-$PtBOS_{113}$ diblock copolymer had a diameter of around 30 nm with a narrow size distribution. The PS_{48}-*b*-$PtBOS_{113}$/$PtBOS_{28}$ blend with 10% *w*/*w* $PtBOS_{28}$ homopolymer resulted in a similar size. In the case of the 30% *w*/*w* $PtBOS_{28}$ homopolymer, the mixture of spherical and worm-like nano-objects showed an average size of about 100 nm with a broad size distribution. In the cases with 50% *w*/*w* $PtBOS_{28}$ homopolymer, the average size of vesicular nano-objects reached approximately 600 nm. On further increasing the $PtBOS_{28}$ homopolymer content to 60% *w*/*w*, 70% *w*/*w*, and 80% *w*/*w*, the vesicles gradually formed, merged, and evolved, and nano-objects with larger sizes could be discriminated. Overall, with the increase of the $PtBOS_{28}$ homopolymer content, the TEM images depicted a gradual evolution from spherical to worm-like, vesicular, and sponge-like morphologies, and the DLS curves showed a regular increasing tendency of the sizes. Both measurements contributed to consistent results.

Subsequently, using the $PtBOS_{28}$ homopolymer as an additive, the MICA process was further studied by varying DP_{PtBOS} in PS-*b*-PtBOS diblock copolymers (or DP_{PHOS} in PS-*b*-PHOS diblock copolymers). When the $PtBOS_{28}$ homopolymer content was fixed at 10% *w*/*w*, the MICA process of PS_{48}-*b*-$PtBOS_{113}$/$PtBOS_{28}$, PS_{48}-*b*-$PtBOS_{170}$/$PtBOS_{28}$, PS_{48}-*b*-$PtBOS_{220}$/$PtBOS_{28}$, and PS_{48}-*b*-$PtBOS_{287}$/$PtBOS_{28}$ blends generated spherical, worm-like, vesicular and vesicular morphologies (Figure 4a−d), respectively. These morphologies resembled those observed in the MISA process of PS_{48}-*b*-$PtBOS_{113}$, PS_{48}-*b*-$PtBOS_{170}$, PS_{48}-*b*-$PtBOS_{220}$, and PS_{48}-*b*-$PtBOS_{287}$ diblock copolymers without the addition of a $PtBOS_{28}$ homopolymer (Figure 2b−e). Differently, the worm-like and vesicular morphologies in the MICA system were slightly merged and fused. Prominently, when the $PtBOS_{28}$ homopolymer content was increased to 30% *w*/*w*, the MICA of the PS_{48}-*b*-$PtBOS_{113}$/$PtBOS_{28}$ blend generated a mixture of spherical and worm-like morphologies (Figure 4e). The MICA of the PS_{48}-*b*-$PtBOS_{170}$/$PtBOS_{28}$ blend evolved into a vesicular morphology (Figure 4f), which was similar to that from the PS_{48}-*b*-$PtBOS_{220}$/$PtBOS_{28}$ blend (Figure 4g). The MICA of the PS_{48}-*b*-$PtBOS_{287}$/$PtBOS_{28}$ blend formed a sponge-like morphology (Figure 4h). When the $PtBOS_{28}$ homopolymer content was continuously increased to 50% *w*/*w*, both the MICA of PS_{48}-*b*-$PtBOS_{113}$/$PtBOS_{28}$ and PS_{48}-*b*-$PtBOS_{170}$/$PtBOS_{28}$ blends evolved into vesicular morphologies (Figure 4i,j). The MICA of the PS_{48}-*b*-$PtBOS_{220}$/$PtBOS_{28}$ blend shifted to the sponge-like morphology (Figure 4k). However, the MICA of PS_{48}-*b*-$PtBOS_{287}$/$PtBOS_{28}$ blend generated the precipitate, and the dispersion could not be maintained (Figure 4l).

Furthermore, besides the above $PtBOS_{28}$, the effect of DP_{PtBOS} of the PtBOS homopolymer (or DP_{PHOS} of the PHOS homopolymer) on the MICA process of PS-*b*-PtBOS/PtBOS blends was further investigated. The PtBOS homopolymer content was first fixed as 30% w/w, and DP_{PtBOS}s of PtBOS homopolymers were varied. As shown in Figure 5, a mixture of spherical and short worm-like morphologies (Figure 5a), composites of worm-like and vesicular morphologies (Figure 5b), and vesicular morphologies (Figure 5c,d) were observed in the MICA process of PS_{48}-*b*-$PtBOS_{113}$/$PtBOS_{13}$, PS_{48}-*b*-$PtBOS_{170}$/$PtBOS_{13}$, PS_{48}-*b*-$PtBOS_{220}$/$PtBOS_{13}$, and PS_{48}-*b*-$PtBOS_{287}$/$PtBOS_{13}$. Obviously, the spherical morphology from the MISA process of PS_{48}-*b*-$PtBOS_{113}$ (Figure 2b) evolved into a mixture of spherical and short worm-like morphologies (Figure 5a), and the worm-like morphology in PS_{48}-*b*-$PtBOS_{170}$ (Figure 2c) evolved into a composite of worm-like and vesicular morphologies in the MICA process (Figure 5b). PS_{48}-*b*-$PtBOS_{220}$/$PtBOS_{13}$ and PS_{48}-*b*-$PtBOS_{287}$/$PtBOS_{13}$ maintained the vesicular morphologies (Figure 5c,d) as those in PS_{48}-*b*-$PtBOS_{220}$ and PS_{48}-*b*-$PtBOS_{287}$ (Figure 2d,e). When $PtBOS_{28}$ was introduced, after the MICA process, PS_{48}-*b*-$PtBOS_{113}$/$PtBOS_{28}$ maintained a mixture of spherical and short worm-like morphologies (Figure 5e), and PS_{48}-*b*-$PtBOS_{220}$/$PtBOS_{28}$ retained a vesicular morphology (Figure 5g). After the MICA process, PS_{48}-*b*-$PtBOS_{170}$/$PtBOS_{28}$ was completely converted into vesicular morphology (Figure 5f), and PS_{48}-*b*-$PtBOS_{287}$/$PtBOS_{28}$ was partially evolved into sponge-like morphology (Figure 5h). When $PtBOS_{52}$ was introduced, after the MICA process, PS_{48}-*b*-$PtBOS_{113}$/$PtBOS_{112}$ and PS_{48}-*b*-$PtBOS_{170}$/$PtBOS_{112}$ maintained spherical and vesicular morphologies (Figure 5i,j), respectively. PS_{48}-*b*-$PtBOS_{220}$/$PtBOS_{52}$ was partially converted into sponge-like morphology (Figure 5k), and PS_{48}-*b*-$PtBOS_{287}$/$PtBOS_{52}$ was completely converted into sponge-like morphology (Figure 5l). Furthermore, when $PtBOS_{112}$ was introduced, after the MICA process, PS_{48}-*b*-$PtBOS_{113}$/$PtBOS_{112}$ and PS_{48}-*b*-$PtBOS_{170}$/$PtBOS_{112}$ still maintained spherical and vesicular morphologies (Figure 5m,n), respectively. The MICA process of PS_{48}-*b*-$PtBOS_{220}$/$PtBOS_{52}$ and PS_{48}-*b*-$PtBOS_{220}$/$PtBOS_{112}$ completely converted them into sponge-like morphologies (Figure 5o,p).

Alternatively, at a PtBOS homopolymer content of 50% *w*/*w*, the effect of DP_{PtBOS} on the PtBOS homopolymer (or DP_{PHOS} on the PHOS homopolymer) on morphological evolution was also investigated. As shown in Figure 6, a mixture of spherical and short worm-like (Figure 6a), vesicular (Figure 6b,c), and sponge-like (Figure 6d) morphologies were observed upon the MICA process of PS_{48}-*b*-$PtBOS_{113}$/$PtBOS_{13}$, PS_{48}-*b*-$PtBOS_{170}$/$PtBOS_{13}$, PS_{48}-*b*-$PtBOS_{220}$/$PtBOS_{13}$, and PS_{48}-*b*-$PtBOS_{287}$/$PtBOS_{13}$. In these cases, the spherical morphology in the MISA of PS_{48}-*b*-$PtBOS_{113}$ (Figure 2b) evolved into a mixture of sphere and short worm-like morphologies in the MICA of PS_{48}-*b*-$PtBOS_{113}$/$PtBOS_{13}$ (Figure 6a), and the worm-like morphology in the MISA of PS_{48}-*b*-$PHOS_{170}$ (Figure 2c) evolved into a thin-wall vesicular one in the MICA of PS_{48}-*b*-$PtBOS_{170}$/$PtBOS_{13}$ (Figure 6b). The MICA of PS_{48}-*b*-$PtBOS_{220}$/$PtBOS_{13}$ maintained a thick-wall vesicular morphology (Figure 6c) as that of the MISA of PS_{48}-*b*-$PtBOS_{220}$ (Figure 2d). Uniquely, different from the vesicular morphology in the MISA process of PS_{48}-*b*-$PtBOS_{287}$ (Figure 2e), the sponge-like morphology was completely formed in the MICA of PS_{48}-*b*-$PtBOS_{287}$/$PtBOS_{13}$ (Figure 6d). Unlike the case with a PtBOS homopolymer content of 30% *w*/*w*, herein, the introduction of $PtBOS_{13}$ with a higher PtBOS homopolymer content (50% *w*/*w*) could significantly modulate the morphological evolution of nano-objects. Continu-

https://doi.org/10.1021/acs.macromol.5c02207
Macromolecules 2025, 58, 11123−11136

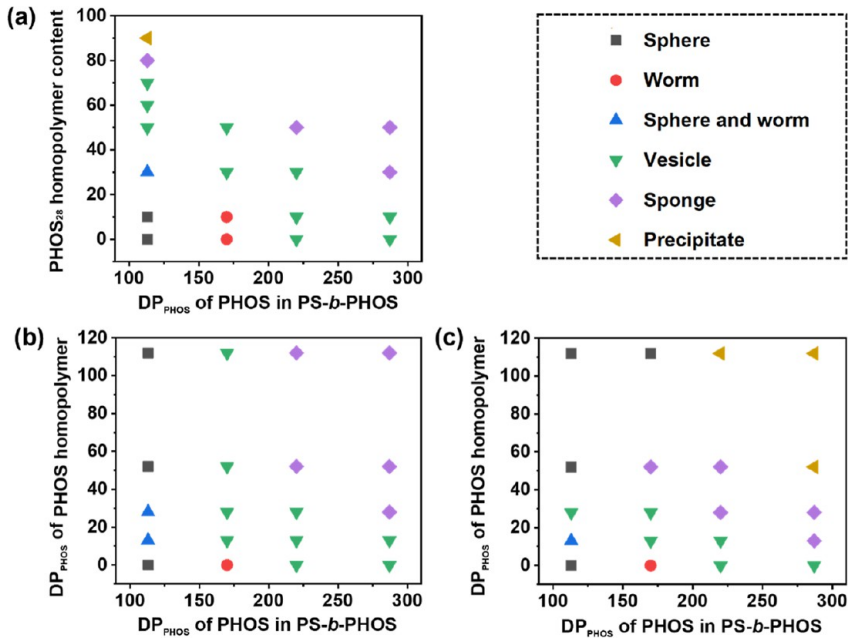

Figure 7. Morphological distribution of nano-objects in MISA or MICA processes: (a) with different DP_{PHOS} in PS-*b*-PHOS diblock copolymers and $PHOS_{28}$ homopolymer contents, (b) with different DP_{PHOS} in PS-*b*-PHOS diblock copolymers and 30% *w*/*w* PHOS homopolymer content, and (c) with different DP_{PHOS} in PS-*b*-PHOS diblock copolymers and 50% *w*/*w* PHOS homopolymer content.

ously, when $PHOS_{28}$ was introduced, the MICA process of PS_{48}-*b*-P*t*BOS$_{113}$/P*t*BOS$_{28}$ converted it into vesicular morphology (Figure 6e), PS_{48}-*b*-P*t*BOS$_{170}$/P*t*BOS$_{28}$ maintained a vesicular morphology (Figure 6f), and PS_{48}-*b*-P*t*BOS$_{220}$/P*t*BOS$_{28}$ completely evolved into sponge-like morphology (Figure 6g). When $PHOS_{52}$ was introduced, the MICA process of PS_{48}-*b*-P*t*BOS$_{113}$/P*t*BOS$_{52}$ turned it back to the sphere morphology (Figure 6i), and PS_{48}-*b*-P*t*BOS$_{170}$/P*t*BOS$_{52}$ and PS_{48}-*b*-P*t*BOS$_{220}$/P*t*BOS$_{52}$ were completely converted into sponge-like morphologies (Figure 6j,k). When P*t*BOS$_{112}$ was introduced, after the MICA process, PS_{48}-*b*-P*t*BOS$_{113}$/P*t*BOS$_{112}$ maintained a spherical morphology (Figure 6m), and PS_{48}-*b*-P*t*BOS$_{170}$/P*t*BOS$_{112}$ was also lowered as a spherical morphology (Figure 6n). Especially, in the case of 50% *w*/*w* P*t*BOS homopolymer, the precipitates were mostly observed in the MICA of PS_{48}-*b*-P*t*BOS$_{220}$/P*t*BOS$_{28}$ (Figure 6h), PS_{48}-*b*-P*t*BOS$_{220}$/P*t*BOS$_{52}$ (Figure 6l), PS_{48}-*b*-P*t*BOS$_{220}$/P*t*BOS$_{112}$ (Figure 6o), and PS_{48}-*b*-P*t*BOS$_{287}$/P*t*BOS$_{112}$ (Figure 6p) blends. As an example, it should be mentioned that the nano-objects formed by the MICA of PS_{48}-*b*-PHOS$_{113}$/PHOS$_{112}$ could be well dispersed as shown in Figure 6m, while the nano-objects formed by the MICA of PS_{48}-*b*-PHOS$_{170}$/PHOS$_{112}$ were severely aggregated as shown in Figure 6n. Even after further dilution of the latter, the aggregates still remained. By analyzing the self-assembly tendency from Figure 6m to p, it could be noticed that the spheres formed and shown in Figure 6n approached the precipitate shown in Figure 6o. That is, the PS_{48}-*b*-PHOS$_{170}$/PHOS$_{112}$ nano-objects could be regarded as a metastable state, which were ready to aggregate and precipitate after a certain standing time. The reason might be due to the increased content of the PHOS core in nano-objects and the reduced stability of the PS shell to the nano-objects.

Interpretation of the Morphological Evolution in MISA or MICA Processes. Based on the above TEM results, the morphological distribution of the MISA or MICA system was depicted with the DP_{PtBOS} of P*t*BOS in the PS-*b*-P*t*BOS diblock copolymer (or DP_{PHOS} of PHOS in the PS-*b*-PHOS diblock copolymer) as the horizontal axis and the P*t*BOS$_{28}$ (or $PHOS_{28}$) homopolymer content as the vertical axis (Figure 7a). Obviously, in the cases with 10% *w*/*w* P*t*BOS$_{28}$ homopolymer content, the morphologies were similar to those without any P*t*BOS$_{28}$ homopolymer. The reason could be attributed to the relatively low P*t*BOS$_{28}$ homopolymer content. However, once the P*t*BOS$_{28}$ homopolymer content surpassed 30% *w*/*w*, the morphologies underwent a prominent evolution tendency. That is, from 0% w/w to 80% w/w of P*t*BOS$_{28}$ homopolymer content, the PS_{48}-*b*-P*t*BOS$_{113}$/P*t*BOS$_{28}$ blends evolved from spherical to a mixture of spherical and short worm-like, sponge-like morphologies, and finally precipitated. From 0% w/w to 50% *w*/*w* P*t*BOS$_{28}$ homopolymer content, the PS_{48}-*b*-P*t*BOS$_{170}$/P*t*BOS$_{28}$ blends evolved from worm-like to vesicular morphologies, and the PS_{48}-*b*-P*t*BOS$_{220}$/P*t*BOS$_{28}$ and PS_{48}-*b*-P*t*BOS$_{287}$/P*t*BOS$_{28}$ blends evolved from vesicular to sponge-like morphologies. Obviously, the addition of the P*t*BOS$_{28}$ homopolymer could significantly modulate the morphological evolution in the MICA process. Generally, the higher-order morphologies, such as vesicles and sponges, were favored in the cases with a higher P*t*BOS$_{28}$ homopolymer content. Similarly, based on the above TEM results in the cases with 30% *w*/*w* (Figure 7b) and 50% *w*/*w* (Figure 7c) P*t*BOS homopolymer content, the morphological distribution was depicted with the DP_{PtBOS} of P*t*BOS in the PS-*b*-P*t*BOS diblock copolymer (or DP_{PHOS} of PHOS in the PS-*b*-PHOS diblock copolymer) as the horizontal axis and the DP_{PtBOS} of the P*t*BOS homopolymer (or DP_{PHOS} of the PHOS homopolymer) as the vertical axis. The P*t*BOS homopolymer with lower MW and higher content tended to contribute to the nano-objects with higher-order morphologies. Oppositely, the higher MW and higher content tended to generate the precipitates. Comparing the morphological distribution at 30% *w*/*w* and 50% *w*/*w* P*t*BOS homopolymer content, it could also be found that the higher P*t*BOS homopolymer content tended to accelerate the morphological

https://doi.org/10.1021/acs.macromol.5c02207
Macromolecules 2025, 58, 11123−11136

Scheme 2. Schematic Illustration of the Morphological Evolution in MISA or MICA Processes

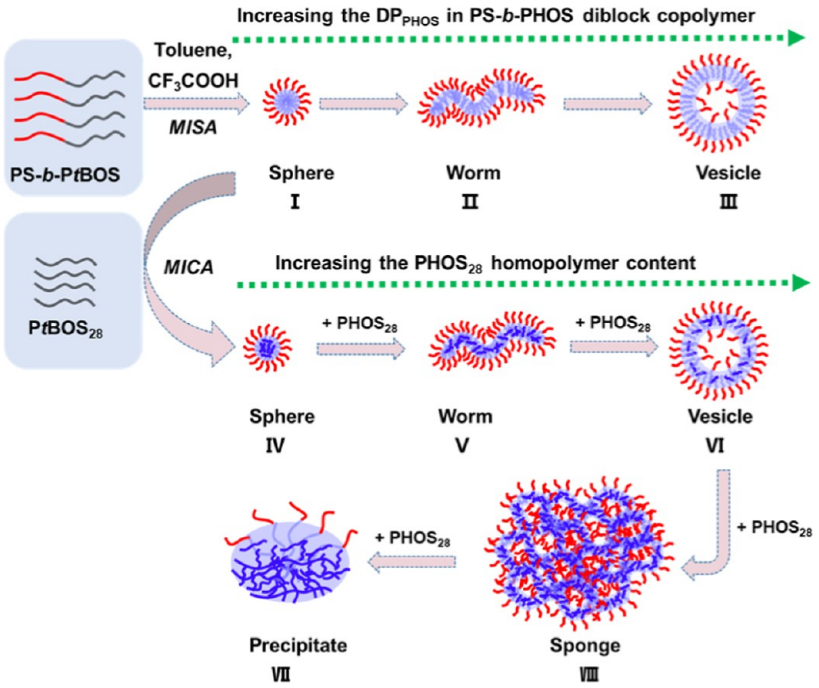

evolution of nano-objects. The reason might be attributed to the fact that the generated PHOS homopolymer with lower MW has relatively good solubility and improved mobility in toluene, which facilitated the cooperative self-assembly of PS-*b*-PHOS and PHOS. Correspondingly, the self-assembly could be sufficiently modulated, and higher-order morphologies were favored. In the cases for the P*t*BOS homopolymer with higher *M*W, the generated PHOS homopolymer had reduced solubility and mobility during the MICA process. The PS shell could not efficiently stabilize the nano-objects, and thus, the precipitate was readily formed.

Following the general principle of self-assembly of block copolymers, the longer core-forming block promoted the evolution of nano-objects into higher-order morphologies. Differently, in the typical PISA process, the core-forming block was gradually extended and prolonged, and the solubility of the core-forming block gradually decreased. In our MISA process, the length of the core-forming block was fixed at the beginning of the self-assembly. Nevertheless, the solubility of the core-forming block also gradually decreased. Thus, the nano-objects in PISA and MISA processes should share a similar morphological evolution tendency. The morphological transformation of block copolymers during the PISA process was generally expressed using the formula $P = V/a_0 l_c$, which was primarily determined by the volume of the nucleated chain segments (V), the surface area of the shelled portion (a_0), and the chain length of the nucleated chain segments (l_c).[8,19,58] Generally, it was assumed that spherical micelles were generated for $P \leq 1/3$, worm-like micelles were obtained for $1/3 < P \leq 1/2$, and vesicular micelles were collected for $1/2 < P \leq 1$. The TEM images in Figure 2 and the morphological distribution in Figure 7a show similar morphological evolution tendencies. As DP$_{PtBOS}$ (or DP$_{PHOS}$) increased, the length of the core-forming block PHOS increased. Correspondingly, the P value was increased, and the nano-objects regularly evolved from spherical (I) to worm-like (II) and vesicular (III) morphologies (Scheme 2).

Alternatively, in the presence of the P*t*BOS homopolymer, upon the addition of the TFA agent, the P*t*BOS in the PS-*b*-P*t*BOS diblock copolymer and the P*t*BOS homopolymer underwent simultaneous conversion into the core-forming PHOS in the MICA process. Both PHOS blocks were stabilized by the PS block. In contrast to the MISA process of the single PS-*b*-PHOS diblock copolymer, the homopolymer PHOS block possesses higher mobility and flexibility, thereby significantly facilitating the generation and progression of the self-assembled morphologies. The parameters including the DP$_{PtBOS}$ and content of the P*t*BOS homopolymer, as well as the DP$_{PtBOS}$ in PS-*b*-P*t*BOS diblock copolymer, could affect the morphological evolution. For example, in the MICA process of PS$_{48}$-*b*-PtBOS$_{113}$/PtBOS$_{28}$, as hydrolysis progressed, the generated PHOS gradually reached its solubility limitation and became insoluble. These insoluble PHOS blocks aggregated and formed an insoluble core, which further adsorbed the PS-*b*-PHOS diblock copolymer. This resulted in a significant increase in the volume of the nucleated chain segments (V) and a decrease in the partially soluble PHOS chain segments (l_c), leading to a substantial increase in the filling parameter P. With the increase of the PHOS homopolymer content, a morphological transition from spherical (I, IV) to worm-like (V), vesicular (VI), and sponge-like (VII) morphologies was observed (Scheme 2). However, when the PtBOS$_{28}$ homopolymer reached 90% *w*/*w*, precipitation finally occurred due to the insufficient solvent-friendly PS block to stabilize the self-assemblies. Similarly, the MICA system with different P*t*BOS homopolymers and PS-*b*-P*t*BOS diblock copolymers followed the same morphological evolution tendency in the case with a DP$_{PtBOS}$ homopolymer content of 30% *w*/*w*. Differently, in the cases with a DP$_{PtBOS}$ homopolymer content of 50% *w*/*w*, the P*t*BOS homopolymer and PS-*b*-P*t*BOS diblock copolymers with higher DP$_{PtBOS}$ promoted the formation of precipitates and caused the failure of the MICA process. The reason might be the enhanced

https://doi.org/10.1021/acs.macromol.5c02207
Macromolecules 2025, 58, 11123−11136

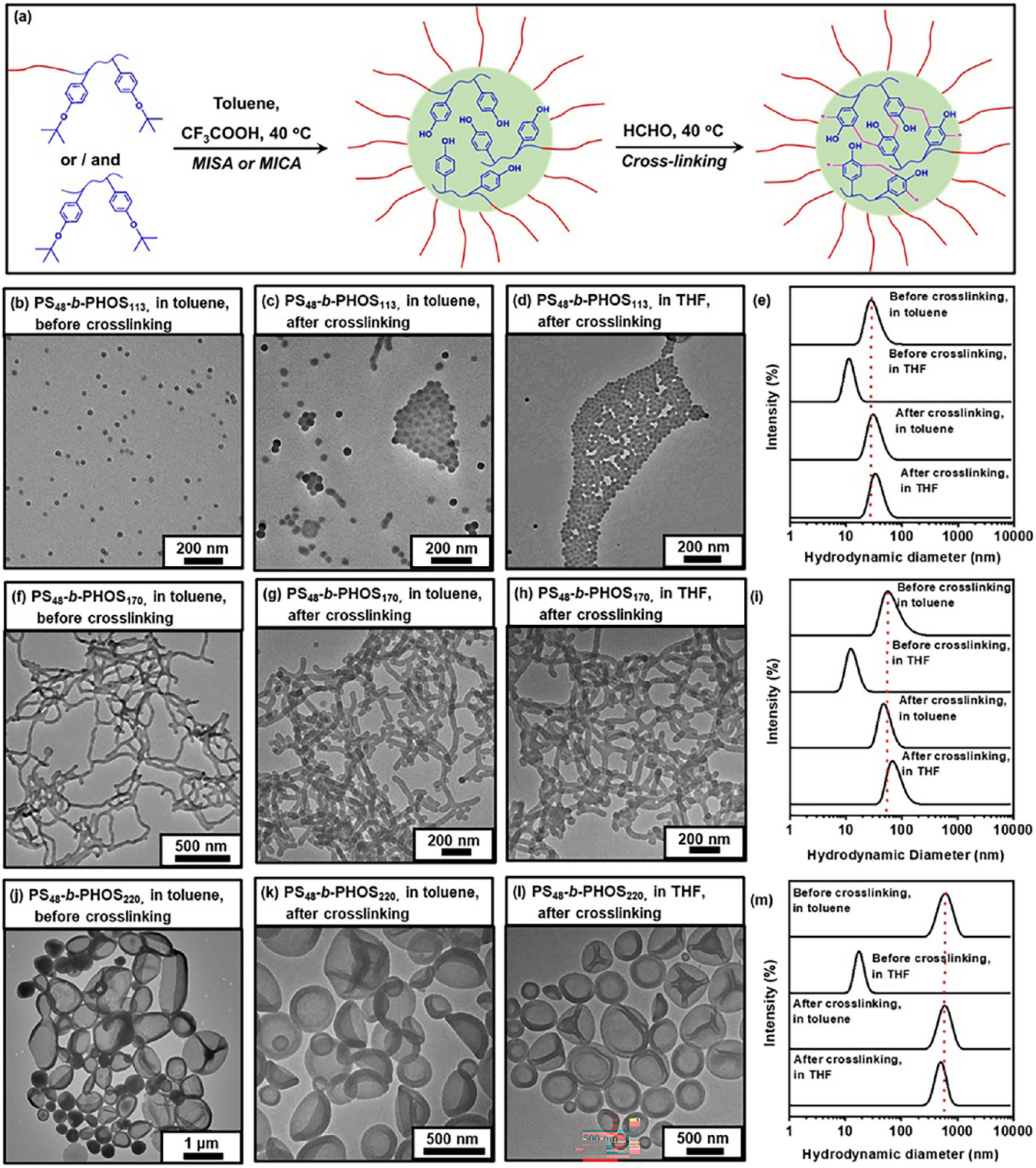

Figure 8. (a) Stabililzation process of the nano-objects by phenol−aldehyde reaction. TEM images of nano-objects (diluted into 0.1−0.3% *w/w*): (b, f, j) dispersed in toluene before cross-linking, (c, g, k) dispersed in toluene after cross-linking with formaldehyde, and (d, h, i) dispersed in THF after cross-linking with formaldehyde. The DLS curves of the corresponding nano-objects dispersed in toluene or THF (e, i, m).

fusion between the higher-order nano-objects, which could not be stabilized by the PS block.

Stabilization of Nano-objects in MISA or MICA Processes. For a certain practical application, maintaining the morphology of nano-objects during the process was a key issue. Herein, for the PS-*b*-PHOS or PS-*b*-PHOS/PHOS nano-objects, the generated PHOS in the core region could be cross-linked by the aldehyde, and the nano-object functionalized with phenolic formaldehyde resin core could be readily achieved. Under acidic conditions, the cross-linking reaction involved the electrophilic aromatic substitution of carbon atoms adjacent to the phenol by the aldehyde, forming hydroxymethyl phenol, which further condensed with another carbon atom adjacent to the phenol and formed the methylene

https://doi.org/10.1021/acs.macromol.5c02207
Macromolecules 2025, 58, 11123−11136

bridges (Figure 8a). As shown in Figure 8, the stabilized spherical, worm-like, and vesicular nano-objects generated from the MISA of PS_{48}-*b*-P*t*BOS$_{113}$, PS_{48}-*b*-P*t*BOS$_{170}$, and PS_{48}-*b*-P*t*BOS$_{220}$, respectively, could be well dispersed in toluene (Figure 8c,g,k), and the morphologies remained the same as those before the cross-linking reaction (Figure 8b,f,j). Especially, the stabilized nano-objects in THF (Figure 8d,h,l), which was a good solvent for both PS and PHOS block, remained the same as those in the toluene solvent. Meanwhile, the DLS analysis showed that the stabilized nano-objects in toluene and THF had similar sizes, which were obviously distinct from the sizes for the PS-*b*-PHOS diblock copolymers in the THF solvent (Figure 8e,i,m). Thus, the TEM and DLS results comprehensively confirmed that the nano-objects had been successfully stabilized, providing a reliable foundation for potential applications.

Furthermore, the thermal stability of the stabilized nano-objects was investigated. For comparison, the thermal stability of PS_{48}-*b*-PHOS$_{113}$ nano-objects cross-linked with different $[HCHO]_0/[Phenol]_0$ ratios was monitored and compared. As shown in Figure 9, for the PS_{48}-*b*-PHOS$_{113}$ diblock copolymer,

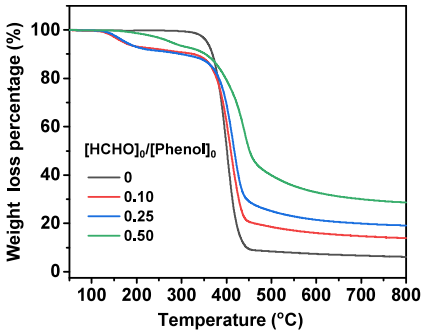

Figure 9. TGA curves of the PS_{48}-*b*-PHOS$_{113}$ nano-objects cross-linked with different $[HCHO]_0/[Phenol]_0$ ratios.

only one weight-loss region between 350 and 450 °C was observed, which was typical for chain breaking and decomposition of the diblock copolymer. For the stabilized PS_{48}-*b*-PHOS$_{113}$ nano-objects, their TGA curves were divided into two weight-loss regions. The weight-loss region between 170 and 350 °C was attributed to the release of formaldehyde and water caused by the further cross-linking/condensation reaction between methylol groups, which accorded with the literature.[59−61] The second weight-loss region occurred mainly between 350 and 450 °C, primarily due to the breakage and decomposition of the main chains. Uniquely, there was a plateau between 450 and 800 °C that could be observed, and only a small portion of weight-loss could be discriminated. The plateau was attributed to the formation of a carbon material and followed the typical TGA behavior of phenolic formaldehyde resin,[62−64] which further indicated the successful cross-linking of phenol groups on PHOS by the aldehyde. Additionally, with the increase of $[HCHO]_0/[Phenol]_0$ ratios, higher degrees of cross-linking were achieved and more residual carbon could be discriminated. The TGA results further confirmed that the phenolic formaldehyde resin core was formed in PS_{48}-*b*-PHOS$_{113}$ nano-objects. Thus, the phenolic formaldehyde resin core not only provided a route to stabilize the nano-objects but also endowed the nano-objects with a potential function in future practical applications, including strengthening the composites, improving the thermal stability, serving as a precursor for nanocarbon, etc.

CONCLUSIONS

In summary, the MISA of PS-*b*-P*t*BOS and MICA of PS-*b*-P*t*BOS/P*t*BOS were realized by employing TFA as a modifying reagent and toluene as a selective solvent. By comprehensive optimization of DP_{PtBOS} in the PS-*b*-P*t*BOS diblock copolymer or P*t*BOS homopolymer, and P*t*BOS homopolymer content, the morphologies could be modulated in a broad window. Besides the typical spherical, worm-like, and vesicular morphologies, the rarely reported sponge-like morphology was also captured in the MICA system. The higher DP_{PtBOS} and higher P*t*BOS homopolymer content promoted the formation of higher-order morphologies. Conveniently, employing the efficient reaction between the phenolic hydroxyl group and formaldehyde, the PHOS core could be cross-linked, and phenolic formaldehyde resin-based nano-objects were generated. The MISA and the derived MICA processes greatly facilitated the preparation of PHOS-based nano-objects. It is hoped that the progress in this contribution can enrich the theory of self-assembly and accelerate the application of functional nano-objects.

ASSOCIATED CONTENT

Supporting Information

The Supporting Information is available free of charge at https://pubs.acs.org/doi/10.1021/acs.macromol.5c02207.

Experimental details and additional characterization data (Figures S1−S4) (PDF)

AUTHOR INFORMATION

Corresponding Author

Guowei Wang − *State Key Laboratory of Molecular Engineering of Polymers, Department of Macromolecular Science, Fudan University, Shanghai 200433, China;* orcid.org/0000-0003-2595-8269; Email: gwwang@fudan.edu.cn

Authors

Peng Zhou − *State Key Laboratory of Molecular Engineering of Polymers, Department of Macromolecular Science, Fudan University, Shanghai 200433, China*

Boyang Shi − *State Key Laboratory of Molecular Engineering of Polymers, Department of Macromolecular Science, Fudan University, Shanghai 200433, China*

Jingwei Zhang − *State Key Laboratory of Molecular Engineering of Polymers, Department of Macromolecular Science, Fudan University, Shanghai 200433, China*

Ding Shen − *State Key Laboratory of Molecular Engineering of Polymers, Department of Macromolecular Science, Fudan University, Shanghai 200433, China*

Di Li − *State Key Laboratory of Molecular Engineering of Polymers, Department of Macromolecular Science, Fudan University, Shanghai 200433, China;* orcid.org/0000-0001-9017-9582

Xinyue Liang − *State Key Laboratory of Molecular Engineering of Polymers, Department of Macromolecular Science, Fudan University, Shanghai 200433, China*

Complete contact information is available at: https://pubs.acs.org/10.1021/acs.macromol.5c02207

https://doi.org/10.1021/acs.macromol.5c02207
Macromolecules 2025, 58, 11123−11136

Notes

The authors declare no competing financial interest.

■ ACKNOWLEDGMENTS

This work is supported by the National Natural Science Foundation of China (22271058).

■ REFERENCES

(1) Mai, Y.; Eisenberg, A. Self-assembly of block copolymers. *Chem. Soc. Rev.* **2012**, *41*, 5969−5985.
(2) Rodríguez-Hernández, J.; Chécot, F.; Gnanou, Y.; Lecommandoux, S. Toward 'smart' nano-objects by self-assembly of block copolymers in solution. *Prog. Polym. Sci.* **2005**, *30*, 691−724.
(3) Shi, B.-Y.; Wang, G.-W. Application of Polymerization-induced Self-assembly (PISA) Technology. *Acta Polym. Sin.* **2022**, *53*, 15−29.
(4) Cheng, X.; Zhang, W. Polymerization-induced Chiral Self-assembly for the In situ Construction, Modulation, Amplification and Applications of Asymmetric Suprastructures. *Angew. Chem., Int. Ed.* **2024**, *63*, No. e202414332.
(5) Yu, W.; Yu, S.; Zhang, X.; Kong, J. Polymerization-induced self-assembly: engineered nanomaterials for advanced biomolecule detection and multifaceted biomedical applications. *J. Polym. Res.* **2025**, *32*, 271.
(6) Cao, J.; Tan, Y.; Chen, Y.; Zhang, L.; Tan, J. Expanding the Scope of Polymerization-Induced Self-Assembly: Recent Advances and New Horizons. *Macromol. Rapid Commun.* **2021**, *42*, 2100498.
(7) Cornel, E. J.; Jiang, J.; Chen, S.; Du, J. Principles and Characteristics of Polymerization-Induced Self-Assembly with Various Polymerization Techniques. *CCS Chem.* **2021**, *3*, 2104−2125.
(8) Gyorgy, C.; Armes, S. P. Recent Advances in Polymerization-Induced Self-Assembly (PISA) Syntheses in Non-Polar Media. *Angew. Chem., Int. Ed.* **2023**, *135*, No. e202308372.
(9) Liu, C.; Hong, C. Y.; Pan, C. Y. Polymerization techniques in polymerization-induced self-assembly (PISA). *Polym. Chem.* **2020**, *11*, 3673−3689.
(10) Serkhacheva, N. S.; Prokopov, N. I.; Lysenko, E. A.; Kozhunova, E. Y.; Chernikova, E. V. Modern Trends in Polymerization-Induced Self-Assembly. *Polymers* **2024**, *16*, 1408.
(11) Wan, J.; Fan, B.; Thang, S. H. RAFT-mediated polymerization-induced self-assembly (RAFT-PISA): current status and future directions. *Chem. Sci.* **2022**, *13*, 4192−4224.
(12) Zhao, Z.; Lei, S.; Zeng, M.; Huo, M. Recent progress in polymerization-induced self-assembly: From the perspective of driving forces. *Aggregate* **2024**, *5*, No. e418.
(13) Zhang, J.; Zhou, P.; Shi, B.; Li, P.; Wang, G. High-Efficient Access to Inverse Morphologies via Living Anionic Polymerization-Mediated Polymerization-Induced Cooperative Assembly. *Macromolecules* **2023**, *56*, 5743−5753.
(14) Zhu, A.; Lv, X.; Shen, L.; Zhang, B.; An, Z. Polymerization-Induced Cooperative Assembly of Block Copolymer and Homopolymer via RAFT Dispersion Polymerization. *ACS Macro Lett.* **2017**, *6*, 304−309.
(15) Huang, C.; Tan, J.; Xu, Q.; He, J.; Li, X.; Liu, D.; Zhang, L. Adding a solvophilic comonomer to the polymerization-induced self-assembly of block copolymer and homopolymer: a cooperative strategy for preparing large compound vesicles. *RSC Adv.* **2017**, *7*, 46069−46081.
(16) Lu, H.; Song, W. Y.; Zou, Y. Y.; Xu, W. S.; Yan, Y. D.; Liu, H.; Ma, L. J. Kinetics and morphologies in polymerization-induced cooperative assembly: a computer simulation investigation. *Polym. Int.* **2022**, *71*, 359−365.
(17) Lv, F.; An, Z.; Wu, P. Efficient Access to Inverse Bicontinuous Mesophases via Polymerization-Induced Cooperative Assembly. *CCS Chem.* **2021**, *3*, 2211−2222.
(18) D'Agosto, F.; Rieger, J.; Lansalot, M. RAFT-Mediated Polymerization-Induced Self-Assembly. *Angew. Chem., Int. Ed.* **2020**, *59*, 8368−8392.
(19) Derry, M. J.; Fielding, L. A.; Armes, S. P. Polymerization-induced self-assembly of block copolymer nanoparticles via RAFT non-aqueous dispersion polymerization. *Prog. Polym. Sci.* **2016**, *52*, 1−18.
(20) Wang, X.; An, Z. New Insights into RAFT Dispersion Polymerization-Induced Self-Assembly: From Monomer Library, Morphological Control, and Stability to Driving Forces. *Macromol. Rapid Commun.* **2019**, *40*, 1800325.
(21) Cao, M.; Zhang, Y.; Wang, J.; Fan, X.; Wang, G. ICAR ATRP Polymerization-Induced Self-Assembly Using a Mixture of Macroinitiator/Stabilizer with Different Molecular Weights. *Macromol. Rapid Commun.* **2019**, *40*, 1900296.
(22) Liang, X.; Zhang, J.; Wu, X.; Fang, X.; Qu, P.; Wang, G. Polyolefin based Nano-Objects via ARGET ATRP mediated Polymerization-Induced Self-Assembly process. *Eur. Polym. J.* **2025**, *230*, 113906.
(23) Petrov, A.; Chertovich, A. V.; Gavrilov, A. A. Phase Diagrams of Polymerization-Induced Self-Assembly Are Largely Determined by Polymer Recombination. *Polymers* **2022**, *14*, 5331.
(24) Shi, B.; Zhang, H.; Liu, Y.; Wang, J.; Zhou, P.; Cao, M.; Wang, G. Development of ICAR ATRP-Based Polymerization-Induced Self-Assembly and Its Application in the Preparation of Organic-Inorganic Nanoparticles. *Macromol. Rapid Commun.* **2019**, *40*, 1900547.
(25) Wang, G.; Wang, Z.; Lee, B.; Yuan, R.; Lu, Z.; Yan, J.; Pan, X.; Song, Y.; Bockstaller, M. R.; Matyjaszewski, K. Polymerization-induced self-assembly of acrylonitrile via ICAR ATRP. *Polymer* **2017**, *129*, 57−67.
(26) Wang, J.; Wu, Z.; Wang, G.; Matyjaszewski, K. In Situ Crosslinking of Nanoparticles in Polymerization-Induced Self-Assembly via ARGET ATRP of Glycidyl Methacrylate. *Macromol. Rapid Commun.* **2019**, *40*, 1800332.
(27) Darabi, A.; Shirin-Abadi, A. R.; Pinaud, J.; Jessop, P. G.; Cunningham, M. F. Nitroxide-mediated surfactant-free emulsion copolymerization of methyl methacrylate and styrene using poly(2-(diethyl)aminoethyl methacrylate-*co*-styrene) as a stimuli-responsive macroalkoxyamine. *Polym. Chem.* **2014**, *5*, 6163−6170.
(28) Lages, M.; Gil, N.; Galanopoulo, P.; Mougin, J.; Lefay, C.; Guillaneuf, Y.; Lansalot, M.; D'Agosto, F.; Nicolas, J. Degradable Vinyl Copolymer Nanoparticles/Latexes by Aqueous Nitroxide-Mediated Polymerization-Induced Self-Assembly. *Macromolecules* **2022**, *55*, 9790−9801.
(29) Qiao, X. G.; Lamber, O.; Taveau, J. C.; Dugas, P. Y.; Charleux, B.; Lansalot, M.; Bourgeat-Lami, E. Nitroxide-Mediated Polymerization-Induced Self-Assembly of Block Copolymers at the Surface of Silica Particles: Toward New Hybrid Morphologies. *Macromolecules* **2017**, *50*, 3797−3807.
(30) Foster, J. C.; Varlas, S.; Blackman, L. D.; Arkinstall, L. A.; O'Reilly, R. K. Ring-Opening Metathesis Polymerization in Aqueous Media Using a Macroinitiator Approach. *Angew. Chem., Int. Ed.* **2018**, *57*, 10672−10676.
(31) Purohit, V. B.; Pieta, M.; Patel, D. M.; Pietrasik, J.; Plummer, C. M. Recent developments in ring-opening metathesis polymerization-induced self-assembly (ROMPISA). *Eur. Polym. J.* **2025**, *223*, 113666.
(32) Sha, Y.; Rahman, M. A.; Zhu, T.; Cha, Y.; McAlister, C. W.; Tang, C. ROMPI-CDSA: ring-opening metathesis polymerization-induced crystallization-driven self-assembly of metallo-block copolymers. *Chem. Sci.* **2019**, *10*, 9782−9787.
(33) Wright, D. B.; Touve, M. A.; Adamiak, L.; Gianneschi, N. C. ROMPISA: Ring-Opening Metathesis Polymerization-Induced Self-Assembly. *ACS Macro Lett.* **2017**, *6*, 925−929.
(34) Zhang, J.; Shi, B.; Wu, X.; Fang, X.; Liang, X.; Peng, Z.; Wang, G. Expanding the Scope of Self-Assembly: Heat-Induced Self-Assembly of Block Copolymers with High Solids. *Macromolecules* **2025**, *58*, 4985−5000.
(35) Guo, G.; Wu, J.; Zhang, J.; Zhou, P.; Shen, D.; Li, P.; Wang, G. Functionalization of nano-objects in living anionic polymerization-induced self-assembly and their use for improving thermal properties of epoxy resins. *Polym. Chem.* **2024**, *15*, 4637−4649.

https://doi.org/10.1021/acs.macromol.5c02207
Macromolecules 2025, 58, 11123−11136

(36) Wang, J.; Cao, M.; Zhou, P.; Wang, G. Exploration of a Living Anionic Polymerization Mechanism into Polymerization-Induced Self-Assembly and Site-Specific Stabilization of the Formed Nano-Objects. *Macromolecules* **2020**, *53*, 3157−3165.
(37) Zhou, C.; Wang, J.; Zhou, P.; Wang, G. A polymerization-induced self-assembly process for all-styrenic nano-objects using the living anionic polymerization mechanism. *Polym. Chem.* **2020**, *11*, 2635−2639.
(38) Huang, F.; Ma, J.; Nie, J.; Xu, B.; Huang, X.; Lu, G.; Winnik, M. A.; Feng, C. A Versatile Strategy toward Donor-Acceptor Nanofibers with Tunable Length/Composition and Enhanced Photocatalytic Activity. *J. Am. Chem. Soc.* **2024**, *146*, 25137−25150.
(39) Shi, B. Y.; Shen, D.; Li, W.; Wang, G. W. Self-Assembly of Copolymers Containing Crystallizable Blocks: Strategies and Applications. *Macromol. Rapid Commun.* **2022**, *43*, 2200071.
(40) MacFarlane, L.; Zhao, C. Q.; Cai, J. D.; Qiu, H. B.; Manners, I. Emerging applications for living crystallization-driven self-assembly. *Chem. Sci.* **2021**, *12*, 4661−4682.
(41) Ma, J. Y.; Lu, G. L.; Huang, X. Y.; Feng, C. π-Conjugated-polymer-based nanofibers through living crystallization-driven self-assembly: preparation, properties and applications. *Chem. Commun.* **2021**, *57*, 13259−13274.
(42) Tao, D.; Wang, Z.; Huang, X.; Tian, M.; Lu, G.; Manners, I.; Winnik, M. A.; Feng, C. Continuous and Segmented Semiconducting Fiber-like Nanostructures with Spatially Selective Functionalization by Living Crystallization-Driven Self-Assembly. *Angew. Chem., Int. Ed.* **2020**, *59*, 8232−8239.
(43) Gwyther, J.; Gilroy, J. B.; Rupar, P. A.; Lunn, D. J.; Kynaston, E.; Patra, S. K.; Whittell, G. R.; Winnik, M. A.; Manners, I. Dimensional Control of Block Copolymer Nanofibers with a -Conjugated Core: Crystallization-Driven Solution Self-Assembly of Amphiphilic Poly(3-hexylthiophene)-b-poly(2-vinylpyridine). *Chem.−Eur. J.* **2013**, *19*, 9186−9197.
(44) Tao, D.; Feng, C.; Cui, Y.; Yang, X.; Manners, I.; Winnik, M. A.; Huang, X. Monodisperse Fiber-like Micelles of Controlled Length and Composition with an Oligo(*p*-phenylenevinylene) Core via "Living" Crystallization-Driven Self-Assembly. *J. Am. Chem. Soc.* **2017**, *139*, 7136−7139.
(45) Zhou, P.; Shi, B.; Liu, Y.; Li, P.; Wang, G. Exploration of the modification-induced self-assembly (MISA) technique and the preparation of nano-objects with a functional poly(acrylic acid) core. *Polym. Chem.* **2022**, *13*, 4186−4197.
(46) Sweat, D. P.; Kim, M.; Schmitt, A. K.; Perroni, D. V.; Fry, C. G.; Mahanthappa, M. K.; Gopalan, P. Phase Behavior of Poly(4-hydroxystyrene-*block*-styrene) Synthesized by Living Anionic Polymerization of an Acetal Protected Monomer. *Macromolecules* **2014**, *47*, 6302−6310.
(47) Tung, P. H.; Kuo, S. W.; Chan, S. C.; Hsu, C. H.; Wang, C. F.; Chang, F. C. Micellization and the surface hydrophobicity of amphiphilic poly(vinylphenol)-*block*-polystyrene block copolymers. *Macromol. Chem. Phys.* **2007**, *208*, 1823−1831.
(48) Chen, X.; Jankova, K.; Kops, J.; Batsberg, W. Hydrolysis of 4-acetoxystyrene polymers prepared by atom transfer radical polymerization. *J. Polym. Sci., Part A: Polym. Chem.* **1999**, *37*, 627−633.
(49) Gao, B.; Chen, X.; Iván, B.; Kops, J.; Batsberg, W. Living atom transfer radical polymerization of 4-acetoxystyrene. *Macromol. Rapid Commun.* **1997**, *18*, 1095−1100.
(50) Natalello, A.; Tonhauser, C.; Frey, H. Anionic Polymerization of para-(1-Ethoxy ethoxy)styrene: Rapid Access to Poly(p-hydroxystyrene) Copolymer Architectures. *ACS Macro Lett.* **2013**, *2*, 409−413.
(51) Faber, M.; Hofman, A. H.; Loos, K.; Brinke, G. t. Highly Ordered Structure Formation in RAFT-Synthesized PtBOS-*b*-P4VP Diblock Copolymers. *Macromol. Rapid Commun.* **2016**, *37*, 911−919.
(52) Kanimozhi, C.; Kim, M.; Larson, S. R.; Choi, J. W.; Choo, Y.; Sweat, D. P.; Osuji, C. O.; Gopalan, P. Isomeric Effect Enabled Thermally Driven Self-Assembly of Hydroxystyrene-Based Block Copolymers. *ACS Macro Lett.* **2016**, *5*, 833−838.
(53) Sweat, D. P.; Yu, X.; Kim, M.; Gopalan, P. Synthesis of poly(4-hydroxystyrene)-based block copolymers containing acid-sensitive blocks by living anionic polymerization. *J. Polym. Sci., Part A: Polym. Chem.* **2014**, *52*, 1458−1468.
(54) Kim, J.; Sandoval, R. W.; Dettmer, C. M.; Nguyen, S. T.; Torkelson, J. M. Compatibilized polymer blends with nanoscale or sub-micron dispersed phases achieved by hydrogen-bonding effects: Block copolymer vs blocky gradient copolymer addition. *Polymer* **2008**, *49*, 2686−2697.
(55) Shi, Q.; Zhang, H.; Jiao, J.; Sun, X.; Sun, J.; Xie, Y.; Liu, L.; Chen, H.; Shen, Y.; Hou, G.; Guo, Y.; Zhang, Z. Poly(styrene-*co*-4-hydroxystyrene) nanofiber membrane for highly selective and efficient Rb+ capture from high salinity solution. *Sep. Purif. Technol.* **2023**, *312*, 123334.
(56) Lee, Y. J. Preparation of poly (4-hydroxystyrene) based functional block copolymer through living radical polymerization and its nanocomposite with $BaTiO_3$ for dielectric material. *J. Nanosci. Nanotechnol.* **2009**, *9*, 7161−7166.
(57) Ayothi, R.; Yi; Cao, H. B.; Yueh, W.; Putna, S.; Ober, C. K. Arylonium Photoacid Generators Containing Environmentally Compatible Aryloxyperfluoroalkanesulfonate Groups. *Chem. Mater.* **2007**, *19*, 1434−1444.
(58) Canning, S. L.; Smith, G. N.; Armes, S. P. A Critical Appraisal of RAFT-Mediated Polymerization-Induced Self Assembly. *Macromolecules* **2016**, *49*, 1985−2001.
(59) Li, C.; Zhang, J.; Yi, Z.; Yang, H.; Zhao, B.; Zhang, W.; Li, J. Preparation and characterization of a novel environmentally friendly phenol-formaldehyde adhesive modified with tannin and urea. *Int. J. Adhes. Adhes.* **2016**, *66*, 26−32.
(60) Lee, W.-J.; Chang, K.-C.; Tseng, I. M. Properties of phenol-formaldehyde resins prepared from phenol-liquefied lignin. *J. Appl. Polym. Sci.* **2012**, *124*, 4782−4788.
(61) Yi, Z.; Li, C.; Jiang, J.; Zhang, J.; Zhang, W.; Li, J. Pyrolysis kinetics of tannin-phenol-formaldehyde resin by non-isothermal thermogravimetric analysis. *J. Therm. Anal. Calorim.* **2015**, *121*, 867−876.
(62) Jiang, H.; Wang, J.; Wu, S.; Wang, B.; Wang, Z. Pyrolysis kinetics of phenol-formaldehyde resin by non-isothermal thermogravimetry. *Carbon* **2010**, *48*, 352−358.
(63) Perez, J. M.; Fernandez, A. Thermal stability and pyrolysis kinetics of lignin-phenol-formaldehyde resins. *J. Appl. Polym. Sci.* **2012**, *123*, 3036−3045.
(64) Yi, Z.; Li, C.; Jiang, J.; Zhang, J.; Zhang, W.; Li, J. Pyrolysis kinetics of tannin-phenol-formaldehyde resin by non-isothermal thermogravimetric analysis. *J. Therm. Anal. Calorim.* **2015**, *121*, 867−876.

https://doi.org/10.1021/acs.macromol.5c02207
Macromolecules 2025, 58, 11123−11136